



Remotely-sensed L4 SST underestimates the thermal fingerprint of coastal upwelling

Claudia Meneghesso^{a,b}, Rui Seabra^a, Bernardo R. Broitman^c, David S. Wethey^d, Michael T. Burrows^e, Benny K.K. Chan^f, Tamar Guy-Haim^g, Pedro A. Ribeiro^{h,1}, Gil Rilov^g, António M. Santos^{a,b}, Lara L. Sousaⁱ, Fernando P. Lima^{a,*}

^a CIBIO, Centro de Investigação em Biodiversidade e Recursos Genéticos, Universidade do Porto, Campus Agrário de Vairão, 4485-661 Vairão, Portugal

^b Faculdade de Ciências da Universidade do Porto, Rua do Campo Alegre s/n, 4169-007 Porto, Portugal

^c Departamento de Ciencias, Facultad de Artes Liberales & Bioengineering Innovation Center, Facultad de Ingeniería y Ciencias, Universidad Adolfo Ibañez, Padre Hurtado 750, Viña del Mar, Chile

^d Department of Biological Sciences, University of South Carolina, Coker Life Sciences Building, 715 Sumter Street, Columbia, SC 29208, USA

^e SAMS, Scottish Association for Marine Science, Oban, Argyll PA37 1QA, Scotland, UK

^f Biodiversity Research Center, Academia Sinica, 128 Academia Road, Sec. 2, Nankang, Taipei 11529, Taiwan

^g National Institute of Oceanography, Israel Oceanographic and Limnological Research (IOLR), PO Box 8030, Haifa 31080, Israel

^h MARE – Marine and Environmental Sciences Centre/IMAR – Instituto do Mar/Centro OKEANOS, Universidade dos Açores, Horta, Portugal

ⁱ Wildlife Conservation Research Unit, Department of Zoology, University of Oxford, The Recanati-Kaplan Centre, Tubney OX13 5QL, UK

ARTICLE INFO

Edited by: Menghua Wang

Keywords:

Sea surface temperature

GHRSSST

Upwelling

Coast

ABSTRACT

Sea Surface Temperature (SST) is an essential variable for understanding key physical and biological processes. Blended and interpolated L4 SST products offer major advantages over alternative SST data sources due to their spatial and temporal completeness, yet their ability to discriminate upwelling-induced steep temperature transitions in coastal waters remains largely unassessed. Here we analysed the performance of eleven L4 GHRSSST-compliant products in estimating *in situ* water temperatures recorded by a large network of shallow subtidal and intertidal temperature loggers deployed in shores covering regimes with a wide range of upwelling intensities. Results indicate that while most products perform satisfactorily for most of the year, performance is severely affected during the upwelling season in locations with strong upwelling. We show that upwelling negatively impacts all four metrics used to assess dataset performance (average bias, correlation, centred root-mean-square error and normalized standard deviation), leading to a considerable overestimation of coastal water temperatures (with average bias exceeding 2 °C in some cases). We also show that while the use of L3 data (i. e., prior to blending and interpolation) leads to an increase in performance compared to L4 GHRSSST-compliant products, the gain is probably not substantial enough to offset issues related with their spatial and temporal inconsistency along coastlines. Our results suggest that the use of L4 GHRSSST-compliant products can lead to a misrepresentation of the thermal fingerprint of upwelling, and thus should be limited (or even avoided) in locations dominated by its effects. Conversely, the use of L4 GHRSSST-compliant products on locations with little to no upwelling appears to be warranted. The mismatch between *in situ* and remotely-sensed sea water temperatures here reported also highlights the need for implementation of long-term monitoring networks of *in situ* temperature loggers.

1. Introduction

Sea Surface Temperature (SST) data are widely used in the fields of

numerical weather prediction, ecological forecasting and climate variability and change. Remotely-sensed SST data are typically delivered as Level 2 products (data sampled on the grid or swath of the

* Corresponding author.

E-mail addresses: meneghesso@claudia@gmail.com (C. Meneghesso), ruisea@gmail.com (R. Seabra), bernardo.broitman@uai.cl (B.R. Broitman), wethey@biol.sc.edu (D.S. Wethey), michael.burrows@sams.ac.uk (M.T. Burrows), chankk@gate.sinica.edu.tw (B.K.K. Chan), tamar.guy-haim@ocean.org.il (T. Guy-Haim), Pedro.Ribeiro@uib.no (P.A. Ribeiro), rilovg@ocean.org.il (G. Rilov), amsantos@fc.up.pt (A.M. Santos), lara.l.sousa@gmail.com (L.L. Sousa), fplima@gmail.com (F.P. Lima).

¹ Present address: Department of Biological Sciences, University of Bergen. Thormøhlensgate 53A, 5006 Bergen, Norway

<https://doi.org/10.1016/j.rse.2019.111588>

Received 5 August 2019; Received in revised form 20 November 2019; Accepted 29 November 2019

0034-4257/ © 2019 Elsevier Inc. All rights reserved.

sensor, at native resolution; L2), Level 3 products (obtained through re-sampling one or various sources of L2 data on a regular grid, but without spatial interpolation; L3), or Level 4 products (obtained by blending complementary satellite and/or *in situ* observations and using interpolation methods to fill data gaps; L4). Being spatially and temporally complete, L4 products are widely used in oceanography and ecology as they support the identification and characterization of oceanographic processes (Isachsen et al., 2012; Santos et al., 2016; Vazquez-Cuervo et al., 2013; Vazquez-Cuervo et al., 2017), weather extremes (e.g., Hobday et al., 2016), marine heatwaves (Oliver et al., 2017), and allow pinpointing the timing of events (e.g., Lima and Wethey, 2012). Most studies using L4 SST rely on data from The Group for High Resolution Sea Surface Temperature (GHRSSST, www.ghrsst.org, Donlon et al., 2007), an international science team providing a framework for SST data sharing and best practices for data processing. It offers a variety of L4 SST products, each featuring a unique blend of data, associated with a particular interpolation technique, and a specific temporal and spatial resolution.

In comparison with the open ocean, obtaining accurate remotely-sensed estimates of near-shore SST is both difficult and complex (e.g., land contamination, interference from coastal fog, cloud cover or precipitation, and from sea roughness). As a consequence, L4 SST products rely more heavily on interpolation and estimates of the climatological time history at the pixel scale to fill in data gaps at the coast. This problem is potentially aggravated in regions featuring steep temperature gradients associated with coastal upwelling. Upwelling is the uplift of cold and nutrient-rich sub-surface water into the euphotic zone, significantly supporting global fisheries (Pauly and Christensen, 1995), enhancing local biodiversity (Lourenço et al., 2016), and buffering coastal biomes from global warming (Varela et al., 2018; Seabra et al., 2019). Importantly, while several studies have addressed the performance of remotely-sensed products in estimating coastal water temperatures (e.g., Brewin et al., 2018; Castillo and Lima, 2010; Smale and Wernberg, 2009; Smit et al., 2013; Thakur et al., 2018), an explicit assessment of the accuracy with which such products discriminate upwelling-induced steep temperature transitions is still lacking. This is especially urgent as L4 SST products continue to be widely applied in studies covering coastal areas (Baker-Austin et al., 2013; Bates et al., 2018; Castillo et al., 2012; Langlais et al., 2017; Liao et al., 2015; Schlegel et al., 2017; Seabra et al., 2019; Varela et al., 2015). Here, we perform a systematic comparison between L4 GHRSSST-compliant data and direct measurements obtained from a global network of *in situ* loggers to determine (i) which L4 GHRSSST-compliant products is a best proxy for estimating water temperatures at the coast, and (ii) to what extent the accuracy of these products is influenced by the magnitude of coastal upwelling.

2. Materials and methods

2.1. *In situ*/reference temperature data

In situ water temperature was recorded using temperature loggers. Loggers were deployed either at shallow subtidal depths, embedded into concrete slabs, or in the low and mid intertidal, attached to natural rock surfaces. Data were collected between 2006 and 2016 from 42 locations worldwide (including the northeast Atlantic, eastern Mediterranean, southeast and northwest Pacific; Fig. 1), at resolutions ranging from 0.01 °C to 0.5 °C and with sampling frequencies ranging from 20 to 60 min (Table 1).

Locations were monitored for periods ranging from 5 months to > 9 years. Since intertidal loggers are periodically exposed to aerial conditions, water temperature was extracted from the full dataset by retaining only temperature records that were collected during the peak of high tide. Tide heights for all locations with intertidal loggers were obtained using the finite element solution model FES2012 (<http://www.avisio.altimetry.fr/>, Carrère et al., 2013). Furthermore,

temperature records from intertidal loggers were discarded whenever simultaneous readings from sensors deployed in the same location varied by > 0.5 °C, or whenever any single logger registered abrupt changes in temperature (i.e., sequential readings exceeding 0.5 °C/h), to avoid potential contamination from aerial exposure. Finally, for each location, temperatures were averaged from multiple sensors whenever these were available and summarised into daily mean values (the average standard deviation between adjacent loggers was 0.12 °C).

2.2. L4 GHRSSST-compliant products

In total, eleven Level 4 (L4) GHRSSST-compliant products were analysed, each featuring a specific blend of data sources (including remotely-sensed infrared, microwave, buoys, drifting gliders and cruise records), spatial resolution (ranging from 0.01 to 0.25 arcdegrees) and temporal extension (see Table 2 for details).

Complete temperature fields are constructed using different interpolation techniques. Most of the GHRSSST-compliant products here analysed are produced using Optimum Interpolation (OI), with the exception of MUR and K10, which instead are produced using, respectively, wavelet and weighted average techniques. For each studied location, estimates of temperature from all L4 GHRSSST-compliant products were obtained from pixels overlapping the area and period under analysis. Spatial overlap was not possible for some locations when using products with coarser resolution, in which case data from the nearest pixel was used (this procedure is common-practice among marine ecologists; Table S1). Complete temporal overlap was also not always possible (e.g., the AVHRR AMSR OI SST product was not available beyond 2011). In such situations, comparisons were restricted to the periods with temporal overlap between *in situ* and remotely-sensed datasets.

2.3. Upwelling index

To evaluate how accurately L4 GHRSSST-compliant products describe the strong horizontal thermal gradients associated with upwelling areas, locations were ranked according to the magnitude of upwelling conditions (Table 1). We used a modified version of the temperature-based 'integrated anomaly' index described by Tapia et al. (2009), which considers both the duration and the intensity of thermal anomalies associated with the uplift of cold water. The Upwelling Index (UI) for each location was defined as the cold anomaly (i.e., cold bias) between upwelled coastal waters and the warmer offshore waters. Thus, a value of 2 °C indicates that upwelling events, on average, reduced coastal water temperature by 2 °C relative to offshore waters. Coastal water temperatures were directly obtained from *in situ* loggers (see above), and the corresponding offshore temperatures were derived from monthly gridded summaries (average) of the International Comprehensive Ocean-Atmosphere Data Set (ICOADS, <https://icoads.noaa.gov>, Freeman et al., 2017), at one arcdegree resolution. ICOADS data were used because they are based on records from thermal sensors on buoys, vessels and surface drifters and thus are independent from satellite observations, whose performance was the subject of this study. Monthly gridded summaries of ICOADS data are not interpolated or analysed to fill data voids. Given the coarse spatial resolution of ICOADS data, there was a non-trivial mismatch between the latitude of each study location and the central latitude of the corresponding ICOADS offshore grid cell. Thus, linear latitudinal transects ~200 km offshore from each coastline were used to compute linear regressions between monthly ICOADS temperatures and latitude. In Taiwan a distance of ~500 km was used to avoid the Kuroshio current thermal effects. This procedure yielded linear regression estimators that were specific for each location and date, allowing the estimation of monthly offshore SST outside the bulk of the influence of coastal upwelling at each study site. Finally, we computed the mean absolute difference between the daily *in situ* water temperatures and the corresponding

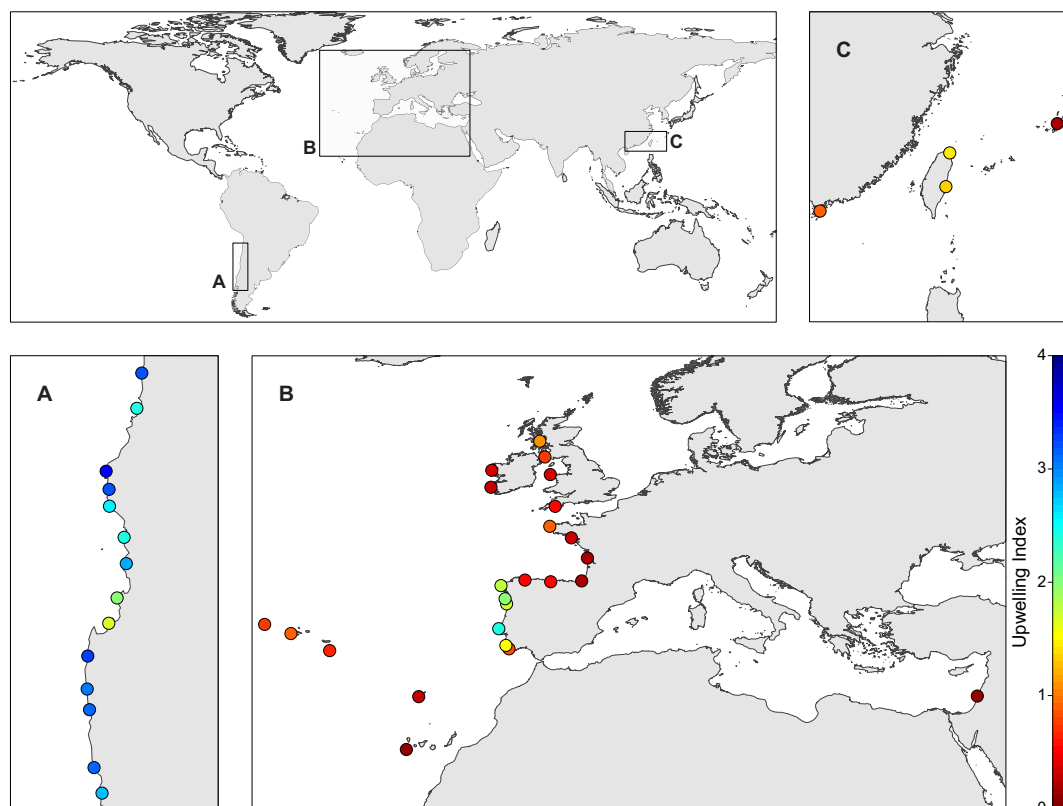


Fig. 1. Location of the 42 coastal sites from which *in situ* temperature data was obtained. Colours show the magnitude of the Upwelling Index at each location (*i.e.*, the cold anomaly between upwelled coastal waters and the warmer offshore waters in °C; see Section 2.3 for further details), ranging from no upwelling (red) to strong upwelling (blue). The magnitude of the cooling effect is strongest in the Chilean locations, followed by those in western Iberia. The remaining locations in the Macaronesia Islands, northeast Atlantic, eastern Mediterranean, Hong Kong, Taiwan and Japan, have weak or no upwelling (*e.g.*, Haifa, Israel). (For interpretation of the references to colour in this figure legend, the reader is referred to the web version of this article.)

latitude-corrected monthly offshore SST whenever coastal waters were cooler (Tapia et al., 2009), yielding a single UI value for each shore.

2.4. Impact of blending methodologies on coastal SST

We also wanted to evaluate to what extent the process used to blend Level 3 (L3) into L4 products could have been introducing artifacts that negatively impact the ability to discriminate sharp temperature transitions near the coast (for example, *via* spatial smoothing during interpolation). L3 data are available at three stages of processing, ranging from uncollated single sensor products to super-collated multi-sensor blends. In this study, we used a high-resolution, GHRSSST-compliant L3C SST dataset (“collated” single sensor, *i.e.*, where multiple measurements from a single sensor are combined into a single product) from the European Organization for the Exploitation of Meteorological Satellites (EUMETSAT), compiled by the Ocean and Sea Ice Satellite Application Facility, France (<http://www.osi-saf.org>) – the Global Metop sub-skin 0.05 arcdegree (~5.55 km) SST dataset on Metop-A satellite (hereafter referred as AVHRR L3 SST). While this product is available twice per day, only night-time SST values from 2009 and 2013 were used for this analysis, to avoid potential interference from diurnal thermal variability associated with solar heating (Donlon et al., 2002; Fairall et al., 1996). These data were also acquired by an Advanced Very High Resolution Radiometer (AVHRR), and thus its performance is comparable to most L4 GHRSSST-compliant blends, which incorporate AVHRR data in their production (see Tables 2 and S2). By comparing the performances of AVHRR L3 SST and L4 GHRSSST-compliant products at estimating *in situ* temperature data we aimed at finding whether (i) L3 and L4 products exhibit biases of the same magnitude, which would suggest that those biases originate during data acquisition and are not

associated with the blending process, or (ii) L3 performs better than L4 products, suggesting that L3 data is preferable to resolve fine temperature patterns near the coast because it does not lose so much detail during the blending process.

2.5. Data analysis

Remotely-sensed GHRSSST-compliant products were evaluated relatively to *in situ* temperature records at two periods: year-round and during the upwelling season. Upwelling seasons were defined as the 6-month time span encompassing the periods of maximum upwelling magnitude, *i.e.*, April to September for the upwelling-dominated shores in Europe (Alvarez et al., 2011; Lafon et al., 2004; Vancamp et al., 1991) and December to May for the Chilean locations. Although the upwelling season along the section off central-northern Chile where *in situ* sensors were located has been described to span from late September to early March (Strub et al., 1998; Tapia et al., 2009), a close inspection of the records for the years 2009–2011 revealed that on those years the magnitude of upwelling was high from December to May, and hence we used that period. This did not change our conclusions (data not shown). While the broad 6-month spans may limit the ability to detect potentially stronger biases associated with peak upwelling conditions, this definition of upwelling seasons was preferred as it ensures a conservative estimate of said biases. The same periods were considered when analysing temperature records from locations with little or no upwelling, warranting consistency among analyses.

The performance of remotely-sensed L4 GHRSSST-compliant datasets was assessed through the computation of: (i) average bias, a measure of their trueness; (ii) Pearson’s correlation coefficient (PCC), indicative of their linear relationship with *in situ* records; (iii) centred root-mean-

Table 1

The performance of remotely-sensed products was assessed by comparing their estimates to direct water temperature measurements (*in situ*) from 42 coastal locations distributed worldwide and collected at timespans varying from 5 months to > 9 years (from Start to End). Temperatures were recorded by loggers (Logger model) deployed in different tidal levels (Level) and depths (Depth; MLWS stands for Mean Low Water Springs and MSL stands for Mean Sea Level), and at different resolutions (Resolution) and frequencies (in minutes; t_x). Daily values were obtained by averaging data collected by one or multiple sensors (N loggers) whenever these were available. *In situ* measurements were also used to calculate an Upwelling Index (UI, in °C) for each location, defined as the magnitude of the cold anomaly (*i.e.*, cold bias) between upwelled coastal waters and the warmer offshore waters (see Tapia et al., 2009). Manufacturer reported logger accuracy was ± 0.21 °C, ± 0.53 °C and 0.50 °C, and logger resolution was 0.02 °C, 0.14 °C and 0.5 °C for Onset TidBit, Hobo Pendant UA00264 and Maxim DS1922 iButton loggers, respectively.

Country	Location	Lat (degrees)	Lon (degrees)	Logger model	t_x (min)	Level	Depth (to datum)	N loggers	Start	End	UI (°C)
Chile	Arrayan	-29.69	-71.32	Onset TidBit	20	Shallow subtidal	1 m below MLWS	1	2009-08-05	2011-11-10	3.2
Chile	Carrizal Bajo	-28.09	-71.16	Onset TidBit	20	Shallow subtidal	1 m below MLWS	1	2009-08-09	2011-11-12	3.6
Chile	Chanaral de Acquituno	-29.07	-71.49	Onset TidBit	20	Shallow subtidal	1 m below MLWS	1	2009-06-26	2011-05-15	3.6
Chile	El Apollillado	-29.21	-71.49	Onset TidBit	20	Shallow subtidal	1 m below MLWS	1	2009-04-26	2011-10-08	2.9
Chile	El Panul	-29.98	-71.38	Onset TidBit	20	Shallow subtidal	1 m below MLWS	1	2009-07-15	2011-10-13	2.2
Chile	Guanaqueros	-30.20	-71.48	Onset TidBit	20	Shallow subtidal	1 m below MLWS	1	2009-08-04	2011-11-08	1.9
Chile	Huasco	-28.38	-71.19	Onset TidBit	20	Shallow subtidal	1 m below MLWS	1	2009-08-08	2011-11-12	2.7
Chile	Huelmelaquien	-31.63	-71.56	Onset TidBit	20	Shallow subtidal	1 m below MLWS	1	2009-08-05	2011-11-07	3.1
Chile	Limari	-30.75	-71.70	Onset TidBit	20	Shallow subtidal	1 m below MLWS	1	2009-03-30	2011-10-10	3.4
Chile	Los Burros	-28.91	-71.52	Onset TidBit	20	Shallow subtidal	1 m below MLWS	1	2009-08-08	2011-11-11	4.0
Chile	Puerto Oscuro	-31.42	-71.60	Onset TidBit	20	Shallow subtidal	1 m below MLWS	1	2009-08-04	2011-11-07	3.5
Chile	Punta Talca	-30.93	-71.68	Onset TidBit	20	Shallow subtidal	1 m below MLWS	1	2009-08-06	2011-11-09	3.5
Chile	Talcaruca	-30.48	-71.70	Onset TidBit	20	Shallow subtidal	1 m below MLWS	1	2009-03-28	2011-11-13	3.6
Chile	Temblador	-29.47	-71.31	Onset TidBit	20	Shallow subtidal	1 m below MLWS	1	2009-08-06	2011-10-12	2.7
England	Wembury	50.31	-4.11	Maxim DS1922 iButton	60	Intertidal	0 to 1 m below MSL	18	2010-06-16	2015-10-29	0.6
France	Batz Sur Mer	47.29	-2.54	Maxim DS1922 iButton	60	Intertidal	0 to 1 m below MSL	18	2010-06-15	2015-10-31	0.3
France	Biarritz	43.48	-1.56	Maxim DS1922 iButton	60	Intertidal	0 to 1 m below MSL	18	2010-06-13	2016-03-09	0.2
France	Landunvez	48.54	-4.75	Maxim DS1922 iButton	60	Intertidal	0 to 1 m below MSL	18	2010-06-17	2015-10-30	1.0
France	Royan	45.61	-1.03	Maxim DS1922 iButton	60	Intertidal	0 to 1 m below MSL	18	2010-06-14	2015-11-01	0.2
Hong Kong	Hong Kong	22.22	114.22	Maxim DS1922 iButton	60	Intertidal	0 to 1 m below MSL	10	2013-05-22	2014-04-16	1.0
Ireland	Emlagh	53.75	-9.91	Maxim DS1922 iButton	60	Intertidal	0 to 1 m below MSL	18	2010-07-16	2016-09-16	0.4
Ireland	Minard Castle	52.13	-10.11	Maxim DS1922 iButton	60	Intertidal	0 to 1 m below MSL	18	2010-07-15	2016-09-17	0.3
Israel	Haifa	32.83	34.95	Hobo Pendant UA00264	60	Shallow subtidal	4 m below MSL	1	2012-03-09	2014-07-07	0.1
Japan	Okinawa	26.55	128.05	Maxim DS1922 iButton	60	Intertidal	0 to 1 m below MSL	5	2015-05-24	2015-10-20	0.2
Portugal	Alteirinhos	37.52	-8.79	Maxim DS1922 iButton	60	Intertidal	0 to 1 m below MSL	18	2010-06-15	2015-12-13	1.7
Portugal	Evaristo	37.07	-8.30	Maxim DS1922 iButton	60	Intertidal	0 to 1 m below MSL	18	2010-06-14	2015-12-12	0.9
Portugal	Faial	38.52	-28.63	Maxim DS1922 iButton	60	Intertidal	0 to 1 m below MSL	5	2013-08-11	2014-07-14	1.0
Portugal	Flores	39.45	-31.12	Maxim DS1922 iButton	60	Intertidal	0 to 1 m below MSL	5	2013-08-20	2014-07-23	0.8
Portugal	Madeira	32.74	-16.69	Maxim DS1922 iButton	60	Intertidal	0 to 1 m below MSL	1	2013-09-23	2014-08-14	0.3
Portugal	Mindelo	41.31	-8.74	Maxim DS1922 iButton	60	Intertidal	0 to 1 m below MSL	18	2010-05-27	2013-05-29	1.9
Portugal	Molede	41.84	-8.87	Maxim DS1922 iButton	60	Intertidal	0 to 1 m below MSL	18	2010-05-27	2016-02-10	2.1
Portugal	Santa Maria	36.94	-25.17	Maxim DS1922 iButton	60	Intertidal	0 to 1 m below MSL	1	2013-08-25	2014-07-29	0.7
Portugal	São Lourenço	39.01	-9.42	Maxim DS1922 iButton	60	Intertidal	0 to 1 m below MSL	18	2010-06-12	2015-12-11	2.7
Scotland	Oban	56.46	-5.45	Maxim DS1921 i-Button	60	Intertidal	0 to 1 m below MSL	3	2006-04-01	2015-05-28	1.2
Scotland	South Cairn	54.97	-5.18	Maxim DS1922 iButton	60	Intertidal	0 to 1 m below MSL	18	2010-07-18	2016-09-19	0.8
Spain	Cabo Touriñán	43.04	-9.29	Maxim DS1922 iButton	60	Intertidal	0 to 1 m below MSL	18	2010-05-29	2016-02-10	2.0
Spain	El Hierro	27.66	-18.02	Maxim DS1922 iButton	60	Intertidal	0 to 1 m below MSL	2	2013-09-17	2014-08-11	0.1
Spain	La Caridad	43.57	-6.83	Maxim DS1922 iButton	60	Intertidal	0 to 1 m below MSL	18	2010-05-30	2016-01-24	0.6
Spain	Prelezo	43.41	-4.44	Maxim DS1922 iButton	60	Intertidal	0 to 1 m below MSL	18	2010-05-31	2016-01-25	0.6
Taiwan	Shi-Ti-Ping	23.48	121.51	Maxim DS1922 iButton	60	Intertidal	0 to 1 m below MSL	14	2013-08-07	2016-04-23	1.5
Taiwan	Shen Ao Keng	25.12	121.82	Maxim DS1922 iButton	60	Intertidal	0 to 1 m below MSL	16	2013-05-29	2016-04-29	1.6
Wales	Isle of Anglesey	53.32	-4.66	Maxim DS1922 iButton	60	Intertidal	0 to 1 m below MSL	18	2010-07-14	2016-09-18	0.4

Table 2
 Eleven Level 4 GHRSSST-compliant products were analysed, each featuring a specific blend of data sources (including remotely-sensed infrared, microwave, buoys, drifting gliders and cruise records, indexed in the Sensor and Platform column and referenced in Table S2), Depth (i.e., the depth to which the dataset refers to; SSTfnd is the temperature at depth, free of diurnal temperature variability), and spatial resolution in arcdegrees (Resolution). The temporal availability (from Start to End) and the number of records used in this study (N records) are also reported.

Product code	Product name	Provider	Source	Depth	Resolution	Start	End	N records	Sensor and Platform
AVHRR AMSR OI	Daily Optimum Interpolation SST(OISST), AMSR+AVHRR	NOAA National Climatic Data Center, USA	https://doi.org/10.5067/GHAOI-4BC01	0.3 m	0.25	2002	2011	21,065	3, 12, 13, 14, 27
AVHRR OI	Daily Optimum Interpolation SST (OISST), AVHRR-Only	NOAA National Climatic Data Center, USA	https://doi.org/10.5067/GHAO-4BC02	0.3 m	0.25	1981	Present	54,916	8, 9, 10, 11, 12, 13, 14, 27
CMCO.2 deg	Canadian Meteorological Centre	Canadian Meteorological Centre, Canada	https://doi.org/10.5067/GHCMC-4FM02	SSTfnd	0.2	1991	Present	54,798	1, 3, 4, 5, 6, 12, 13, 14, 15, 24, 26, 27
GISST	GHRSSST Global 1-km Sea Surface Temperature	NASA Jet Propulsion Laboratory Modelling System, USA	https://doi.org/10.5067/GHGIS-4FP01	SSTfnd	0.01	2010	2017	48,386	3, 6, 18, 19, 21, 22, 24, 27
GAMSSA	Global Australian Multi-Sensor SST Analysis	Australian Bureau of Meteorology, Australia	https://doi.org/10.5067/GHGAM-4FA01	SSTfnd	0.25	2008	Present	53,860	2, 6, 7, 14, 15, 27
GMP K10 SST	Global Ocean SST Multi Product Ensemble Global 10 km Analysed SST	GHRSSST, Group for High Resolution SST Naval Oceanographic Office, USA	http://marine.copernicus.eu/ https://doi.org/10.5067/GHK10-41N01	Ensemble 1 m	0.25 0.1	2009 2008	Present Present	52,392 53,094	Blend of products ^a 3, 6, 14, 15, 16
MUR	Multi-scale Ultra-high Resolution Sea Surface Temperature	NASA Jet Propulsion Laboratory Modelling System, USA	https://doi.org/10.5067/GHGM-4FJ04	SSTfnd	0.01	2002	Present	54,887	3, 14, 19, 20, 26
MW IR OI	Microwave Infrared Optimum Interpolation	Remote Sensing Systems Inc., USA	https://doi.org/10.5067/GHMW-4FR04	SSTfnd	0.09	2005	Present	51,788	2, 3, 19, 20, 24, 26
ODYSSEA	ODYSSEA	IFREMER CERSAT, France	https://doi.org/10.5067/GHGOY-4FE01	SSTfnd	0.02	2010	Present	46,206	1, 3, 13, 14, 23, 24
OSTIA	Operational Sea Surface Temperature and Ice Analysis	UK Meteorological Office, UK	https://doi.org/10.5067/GHOST-4FK01	SSTfnd	0.054	2006	Present	54,446	1, 3, 12, 13, 14, 23, 24, 27

^a AVHRR OI; CMCO.2 deg; The Fleet Numerical Meteorology and Oceanography Center (FNMOC) data, USA; GAMSSA; K10; Merged Satellite and In-situ Data Global Daily SST (MGDSST), Japan Meteorological Agency, Japan SST; OSTIA; ODYSSEA; Microwave/Infrared from Remote Sensing Systems (RSS MW/IR), USA; Microwave from Remote Sensing Systems (RSS MW), USA; Real-Time Global SST (RTG), from the National Centers for Environmental Prediction, USA.

square error (CRMSE), which informs on their accuracy; and (iv) normalized standard deviation (NSD), used to compare their variability with the variability of the data collected *in situ*. To prevent those analyses based on pooled data from becoming dominated by longer time-series, all statistics were estimated using weights, which were computed as the inverse of the length of each timeseries. Taylor diagrams (Taylor, 2001) were used to concisely summarize the degree of correspondence between the suite of satellite-derived datasets and the reference measurements obtained *in situ*. Each Taylor diagram shows, at once, the PCC, CRMSE and NSD of each dataset being evaluated (see Seabra et al., 2011 for an annotated example).

Lastly, to assess the potential impact of biases in remotely-sensed datasets for the calculation of warming trends, *in situ* temperatures were analysed for locations that had timeseries longer than five years. Following Seabra et al. (2019), rates of change in temperature (*i.e.*, the slopes of the linear regressions) were computed for *in situ* temperature records and compared with those based on SST estimates from ten of the L4 GHRSSST-compliant products (AVHRR AMSR OI was excluded from this analysis due to its short temporal overlap with all *in situ* datasets). Only days for which data existed for all combinations of *in situ* and L4 GHRSSST-compliant datasets were retained (1140 days, spanning 5.17 years). All data manipulations and analyses were performed in R (R Core Team, 2018).

3. Results and discussion

When analysing the overall performance of blended L4 GHRSSST-compliant products (*i.e.*, using year-round data from all locations pooled together), we found that most products matched the year-round reference dataset satisfactorily (Fig. 2). The combination of the Pearson's correlation coefficient, the centred root-mean-square error and the normalized standard deviation shows that overall performances ranged from very good when using OSTIA and G1SST (combined PCC = 0.97, CRMSE ≤ 0.26 °C, NSD ≥ 0.96) to good when using AVHRR AMSR OI (PCC = 0.90, CRMSE = 0.44 °C, NSD = 0.94). Despite their good overall performance, average biases associated with each of the

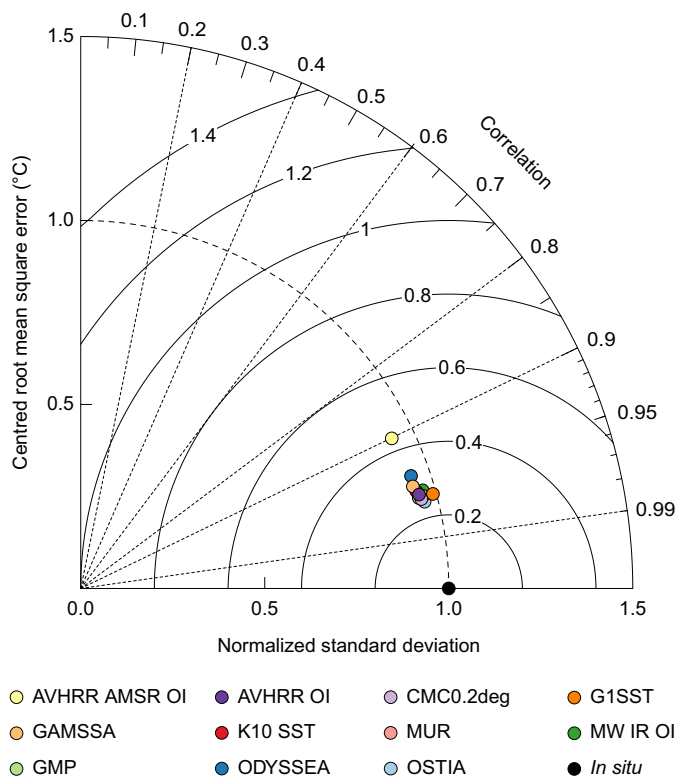


Table 3

Average bias (°C) of L4 GHRSSST-compliant products in estimating coastal water temperatures. A general tendency to overestimation is outlined. The magnitude of positive biases is, however, higher in locations with intense upwelling (UI ≥ 1.7 °C), and especially during the upwelling season, when average biases increase from 0.27 to 0.55 °C (Δ is the increase in average bias from year-round to the upwelling season at locations with strong upwelling). This suggests that the characteristic cold signature of upwelling is underestimated by remotely-sensed products.

L4 GHRSSST-compliant product	Year-round	Year-round	Upwelling season	Δ
	All shores	UI ≥ 1.7	UI ≥ 1.7	
AVHRR AMSR OI	0.69	0.93	1.28	0.35
AVHRR OI	0.61	0.95	1.26	0.31
CMC0.2 deg	0.50	0.86	1.14	0.28
G1SST	0.61	0.81	1.08	0.27
GAMSSA	0.88	1.50	2.05	0.55
GMP	0.67	1.13	1.49	0.36
K10 SST	0.67	1.17	1.59	0.42
MUR	0.55	1.00	1.49	0.49
MW IR OI	0.61	0.97	1.26	0.29
ODYSSEA	0.65	1.19	1.71	0.52
OSTIA	0.43	0.81	1.21	0.40

products indicate that most tend to slightly overestimate water temperatures near the coast (0.43 to 0.88 °C; Table 3), a finding consistent with previous assessments using subtidal loggers (Flores et al., 2018; Smale and Wernberg, 2009).

The second aim of this work was to determine if – and how – the performances of blended L4 GHRSSST-compliant products are influenced by the steep thermal gradients typically originated by upwelling on coastal waters. To that end, we restricted all subsequent analyses to the upwelling season considering the ranking of the locations according to the magnitude of local upwelling conditions. The values obtained for the Upwelling Index were consistent with current knowledge on the global patterns of upwelling (Fig. 1 and Table 1; Chavez and Messié,

Fig. 2. Taylor diagram depicting the overall performance of each of the eleven L4 GHRSSST-compliant products in estimating year-round coastal temperatures at all studied locations at once. The coloured circles are used to distinguish between each L4 GHRSSST-compliant product, while the black circle represents the reference data collected by *in situ* loggers. The azimuth angle of each coloured circle represents its correlation coefficient with the reference dataset, the radial distance from the reference represents the amplitude of its temperature variation, and the resulting CRMSE of each circle is shown by the concentric lines centred on the reference. Most products performed similarly and generally match quite well the year-round reference dataset. It should be noted that the assessment of the worst performing product (AVHRR AMSR OI) was based on a shorter dataset and over a restricted number of locations (see Table 2 for details).

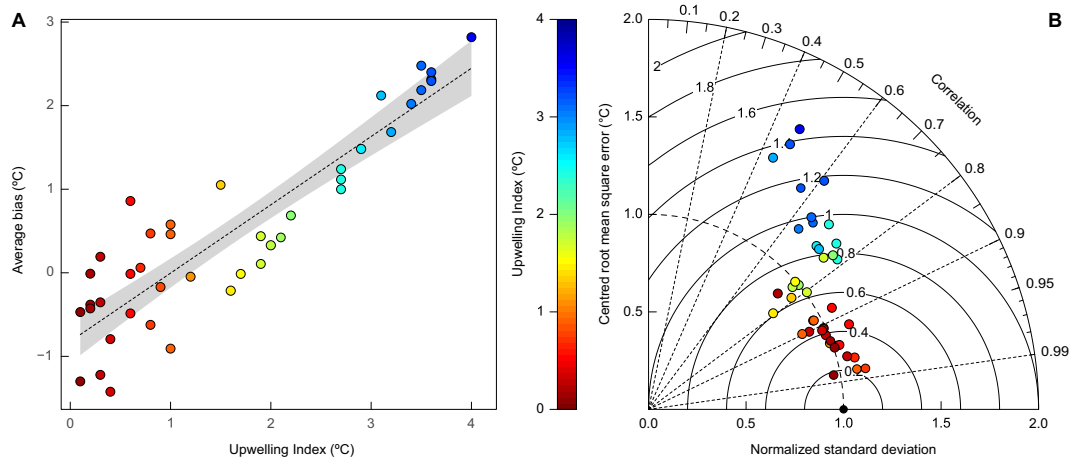


Fig. 3. Combined performance of eleven L4 GHRSSST-compliant products tested in estimating coastal temperatures during the upwelling season at each of the studied locations. Circle colours show the magnitude of upwelling (UI) at each location, from red (no upwelling) to blue (strong upwelling). A – The magnitude of average biases between remotely-sensed products (all pooled together) and *in situ* temperatures increases with upwelling intensity ($R^2 = 0.81$, $f(40) = 175.34$, $p < 0.001$). B – Taylor diagram depicting the combined performance of all L4 GHRSSST-compliant products (excluding AVHRR AMSR OI, excluded from this analysis because it did not overlap with data from some locations). The black circle represents the reference data collected by *in situ* loggers. Estimating *in situ* temperatures using remotely-sensed data is clearly more difficult in locations with stronger upwelling. (For interpretation of the references to colour in this figure legend, the reader is referred to the web version of this article.)

2009; Kämpf and Chapman, 2016). Compared to overall biases (year-round, all shores), biases under the most challenging conditions for remote sensing of coastal SST (*i.e.*, during upwelling season in locations with strong upwelling – UI ≥ 1.7 °C, which includes all shores along the western coast of Iberia and Chile) were substantially greater (1.08 to 2.05 °C; Table 3). The reduced performance associated with upwelling intensity is evident in the Taylor diagram showing the combined efficacy of all L4 GHRSSST-compliant products in estimating *in situ* temperatures at each of the 42 locations studied (Fig. 3B).

This decreased performance of L4 GHRSSST-compliant products was revealed not only through a strong positive link between average bias and upwelling intensity ($R^2 = 0.81$, $f(40) = 175.34$, $p < 0.001$; Fig. 3A), but also through a marked reduction of correlation values (PCC decreasing from a maximum of 0.98 in several locations with no upwelling to a minimum of 0.44 in strong-upwelling Arroyan, Chile), a lowering of accuracy (CRMSE increasing from 0.18 °C in Haifa, Israel, to 1.46 °C at Los Burros, Chile) and an increase of variability (NSD going from 1 in Biarritz, France, to 1.63 in Los Burros, Chile). Additionally, Fig. S1 shows in detail the drop in performance of every single L4 GHRSSST-compliant product across locations with increasing upwelling intensity, suggesting that the overall decrease in performance is pervasive among these datasets, instead of being driven by a subset of particularly bad products. In some extreme conditions, daily estimates of water temperature exceeded those recorded *in situ* by 6 °C (Fig. 4). This large bias is in agreement with peak biases found for upwelling

locations in western South Africa (Smit et al., 2013). It is worth noting that at the other end of the spectrum, at locations with residual upwelling intensity, L4 GHRSSST-compliant products tended to slightly underestimate temperatures, displaying a consistent, albeit small negative bias (low left corner of Fig. 3A).

Although based on a short timespan of around 5 years, the comparison between the warming rates based on *in situ* datasets and on remotely-sensed L4 GHRSSST-compliant products suggests that these tend to overestimate warming, especially in locations with strong upwelling regimes (Fig. S2; $R^2 = 0.16$, $f(158) = 30.03$, $p < 0.001$). This result also suggests that the patterns of reduced warming inside upwelling-dominated regions reported by Seabra et al. (2019) may be underestimated.

Finally, our results also indicate that uninterpolated L3 data (AVHRR L3 SST) can better resolve finer temperature patterns near the coast than any of the blended L4 GHRSSST-compliant products (Fig. 5). Even the direct comparison between G1SST (which was the L4 GHRSSST-compliant product with best performance) and AVHRR L3 SST shows that AVHRR L3 SST estimates better *in situ* temperatures. It has a smaller average bias (0.32 °C, while G1SST has 0.97 °C), a smaller CRMSE (0.64 °C, while G1SST has 0.66 °C) and an NSD closer to the unit (0.96, while G1SST has 1.07), although its correlation with *in situ* measurements is slightly lower (0.78, while G1SST is 0.80).

In situ water temperature measurements were recorded by loggers attached to subtidal or intertidal substrate during high tide (*i.e.*, at a

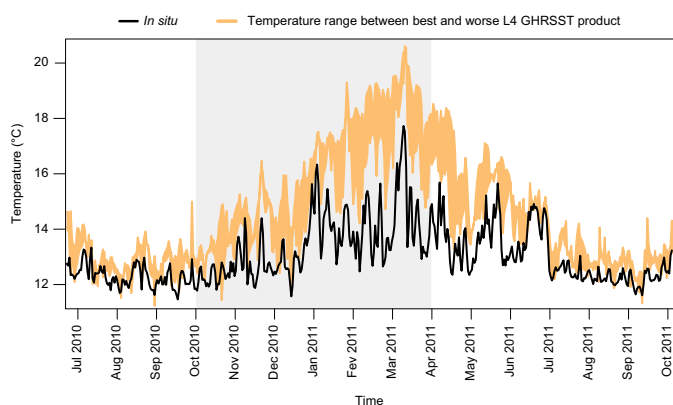


Fig. 4. Comparison between *in situ* measurements (black line) and the range of temperatures estimated by the best (G1SST) and the worst (AVHRR AMSR OI) L4 GHRSSST-compliant products at Los Burros, Chile, the location with the highest upwelling intensity in the current study (UI = 4.02 °C). The mismatch between *in situ* data and the satellite-derived temperature estimates is particularly evident during the upwelling season (grey box; combined average bias between both L4 products and *in situ* data 2.58 °C, PCC 0.58, CRMSE 1.43 °C, NSD 1.59), but is also present outside of the upwelling season to some degree (combined average bias between both L4 products and *in situ* data over the entire period 1.46 °C, PCC 0.78, CRMSE 1.36 °C, NSD 1.88).

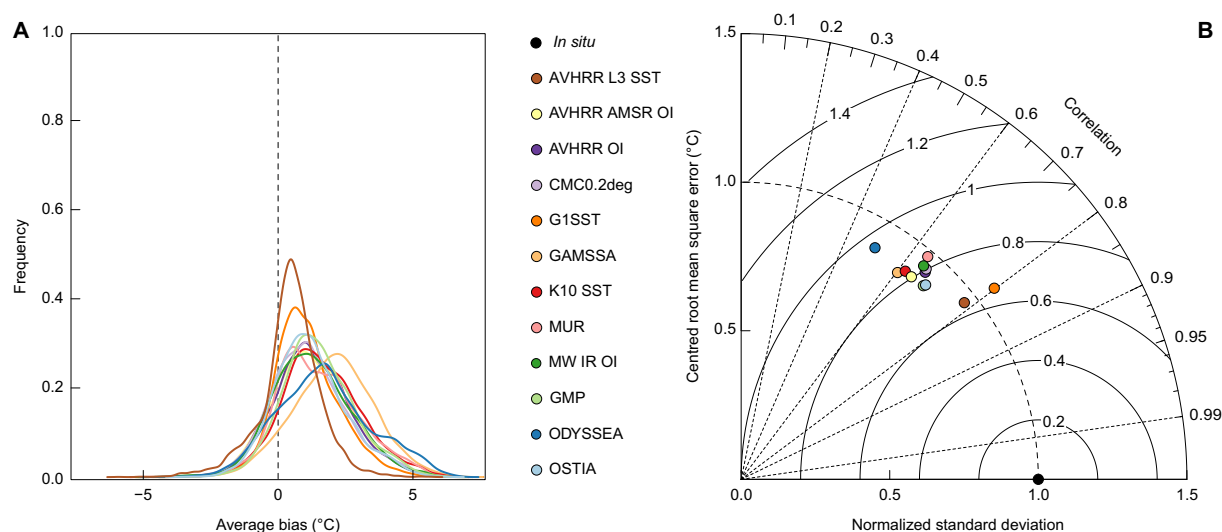


Fig. 5. Comparison between the performance of a L3 SST product (AVHRR L3 SST; brown circle) and the eleven L4 GHRSSST-compliant products tested (remaining coloured circles) in estimating coastal temperatures during the upwelling season at all locations with strongest upwelling ($UI \geq 1.7^\circ\text{C}$; all Chilean and western Iberia shores). A – The shape of the distribution of biases between remotely-sensed products (all pooled together) and *in situ* temperatures highlights a positive (warm) shift in the blended products relative to AVHRR L3 SST. B – Taylor diagram depicting the combined performance of all remotely-sensed products. The black circle represents the reference data collected by *in situ* loggers. Estimating seawater temperatures using L4 GHRSSST-compliant data is clearly more difficult in locations with strong upwelling. AVHRR L3 SST overperforms L4 GHRSSST-compliant data in these situations. (For interpretation of the references to colour in this figure legend, the reader is referred to the web version of this article.)

depth of at least 1 m in all studied locations). These depths differ considerably from the depth of a few mm over which infrared or microwave radiometers acquire data to be subsequently converted into surface temperature. Therefore, one could hypothesise that the observed warm bias of L4 GHRSSST-compliant products when compared with direct measurements *in situ* could have originated from the different depths at which these two datasets were collected across the water column. The validation of this hypothesis is, however, dependent on the verification of several conditions. First, the water column had to be strongly stratified, which is unlikely given the vertical mixing caused by wave action in the surf zone where all loggers were located. Second, the fact that L4 GHRSSST-compliant products show higher bias in locations with stronger upwelling required a stronger stratification in upwelling-dominated locations, which is also unlikely as the wind stress that causes upwelling also promotes the vertical mixing of the water column. It has been shown that wind speeds above 6 ms^{-1} ensure vertical mixing to depths of up to 10 m (Donlon et al., 2002).

Third, the surface skin of the ocean is nearly always cooler than the underlying water because the heat flux is nearly always from the ocean to the atmosphere (Minnett et al., 2011), which would induce a bias in the opposite direction than the warm bias here reported. Still, one could argue that under exceptional conditions (during daytime, at low wind speeds, and under high insolation) a strong thermal stratification could develop (Donlon et al., 2002) and for some unknown reason these conditions occurred more frequently in upwelling-dominated regions. Even then it should not be the cause for the observed warm bias as L4 GHRSSST-compliant datasets are corrected for depth during their production. All L4 GHRSSST-compliant datasets provide temperatures at some sub-surface depth, which in most products is the foundation SST (SST_{fn}), but in some is 0.3 m or 1 m (see Table 2 for details). SST_{fn} is the temperature at depth, free of diurnal temperature variability (Donlon et al., 2002), and thus it should be directly comparable to the bulk temperature measured by the shallow-water loggers in the well-mixed surf zone.

Alternatively, a range of other factors that are specific to coastal regions and to locations with strong upwelling may be intensifying the warm bias found in remotely-sensed coastal temperatures. Firstly, while the spatial interpolation process for pixels farther from the coast can

rely on nearby pixels from all directions, coastal pixels are by definition located at the edges of oceans, and thus interpolation will necessarily result in the imparting of “oceanic” conditions to the coastal pixel. Since the cold thermal fingerprint of upwelling is closely associated with proximity to land (Seabra et al., 2019), this process is likely to result in the attenuation of the cool upwelling signal that is nonetheless captured by *in situ* loggers. Secondly, the impact of land contamination in coastal pixels may be exacerbated by the steep land-sea thermal gradient typically found in locations with strong upwelling (Bakun et al., 2010). Thirdly, high-resolution oceanic temperature data are more likely to be missing at upwelling regions. There are two major classes of satellite-born radiometers used to estimate surface temperature: microwave and infrared (see Table S2). Microwave radiometers such as the Advanced Microwave Scanning Radiometer - Earth Observing System (AMSR-E) aboard the AQUA satellite or the TRMM Microwave Imager (TMI) aboard the TRMM satellite are not sensitive to atmospheric water vapour (such as clouds and fog) but capture data at a coarser spatial resolution (*i.e.*, have footprints of several tens of km) and are strongly affected by land contamination, sea roughness and liquid water (precipitation), which negates their usage at the oceans' margins (up to 50–100 km from the coast). Radiometric data for coastal regions is thus highly dependent on infrared instruments such as the AVHRR aboard most NOAA satellites or the Moderate-Resolution Imaging Spectroradiometer (MODIS) aboard AQUA and TERRA. These infrared radiometers have higher spatial resolution (with footprints of 1 km or less), but infrared transmittance is attenuated by atmospheric water vapour (in the form of fog or clouds). Because fog is positively associated with upwelling (Johnstone and Dawson, 2010), coastal locations with stronger upwelling might be more prone to have missing infrared data, which would further increase the weight of more oceanic pixels during the interpolation process associated with L4 GHRSSST-compliant products. In addition, it is known that the conservative approach followed by current cloud detection algorithms (where in clear areas, in proximity of clouds and steep temperature gradients, valid readings may be misclassified as clouds), often results in discarding cold SST estimates, leading to positive biases over upwelling regions (Derrien et al., 1993; <https://oceancolor.gsfc.nasa.gov/atbd/sst/>). Finally, since shipping routes and buoy deployment locations typically avoid

proximity to the harsh conditions found in the surf zone, correcting for all these factors is further complicated closer to the coast due to a lack of *in situ* temperature readings.

The coastal temperature mismatches identified are complex and hard to model and could have wider implications for the study of the oceanography, biology and ecology of coastal locations, especially within upwelling regions, which are among the most productive coastal areas on the planet (Pauly and Christensen, 1995). Our results show that, while reasonably accurate elsewhere, blended L4 GHRSSST-compliant products fail to properly resolve the thermal environment present in coastal upwelling locations during peak upwelling season. Since the thermal profiles estimated from remote-sensed data and recorded by *in situ* loggers were found to differ substantially in locations with strong upwelling (Figs. 3, 4), and that this mismatch may have been intensified over time (Fig. S2), caution should be taken when interpreting the results from previous trend assessments of coastal sea surface warming (Lima and Wethey, 2012; Rouault et al., 2010; Seabra et al., 2019; Varela et al., 2018) or marine heat wave frequency (Crabbe, 2019; DeCastro et al., 2014; Holbrook et al., 2019) in upwelling locations. Also, even though previous studies have used spatial gradients in temperature derived from L4 GHRSSST-compliant data (and not the absolute temperature values *per se*) to clearly identify upwelling areas (Vazquez-Cuervo et al., 2013; Vazquez-Cuervo et al., 2017), our results suggest that it is also important to validate these methodologies. Furthermore, additional caution is warranted when interpreting assessments of organismal thermal stress levels and the frequency of breaching of upper physiological limits based on L4 data (e.g., King and Sebens, 2018; Seabra et al., 2016), as the magnitude of the biases here reported indicates that they are likely to be overestimations. Importantly, our results also show that, while likely more accurate, even analyses based on L3 data (e.g., Demarcq, 2009; Santos et al., 2012) do not entirely reflect the conditions experienced by coastal organisms (Fig. 5). Thus, in most situations, the increased performance associated with the use of L3 products is unlikely to offset their typical spatial and temporal inconsistency along coastlines, which severely limits their use for analyses requiring long, uninterrupted datasets, (e.g., characterization of marine heat waves).

Taken together, such misrepresentations of the thermal envelope of upwelling locations hinder the understanding of the biogeographic patterns of coastal organisms (Seabra et al., 2015), the identification of cold areas that may provide climate refugia (Rilov et al., 2019; Seabra et al., 2019), the forecasting of climate change impacts (Bates et al., 2018), and downplay the relevance of upwelling regions for the conservation of coastal biodiversity in the context of global warming (Lourenço et al., 2016; Seabra et al., 2019).

The limitations here described regarding the performance of L4 GHRSSST-compliant products in upwelling regions are in-line with those highlighted in the OceanObs19 Community White Paper (O'Carroll et al., 2019). The mismatch between *in situ* water temperatures and remotely-sensed estimates strongly supports the recommendation for an increasing focus on the exploitation of satellite observations in conjunction with *in situ* SST measurements (O'Carroll et al., 2019). Crucially, the sustained implementation of vastly wider monitoring networks of *in situ* coastal temperatures is becoming increasingly feasible, particularly given the relatively reduced cost of maintaining such networks based on collaborative effort, and the recent progress in the development of miniaturized temperature loggers (which now offer higher resilience and autonomy; Judge et al., 2018; Lima et al., 2011).

Author statement

Claudia Meneghesso: Data Curation, Software, Writing - Original Draft and Review and Editing. **Rui Seabra:** Data Curation, Software, Visualization, Writing - Original Draft and Review and Editing, Funding acquisition. **Bernardo R. Broitman:** Conceptualization, Methodology, Data Curation, Writing - Review and Editing, Funding acquisition.

David S. Wethey: Conceptualization, Methodology, Writing - Review and Editing, Funding acquisition. **Michael T. Burrows:** Data Curation, Writing - Review and Editing, Funding acquisition. **Benny K. K. Chan:** Data Curation, Writing - Review and Editing, Funding acquisition. **Tamar Guy-Haim:** Data Curation, Writing - Review and Editing. **Pedro A. Ribeiro:** Data Curation, Writing - Review and Editing, Funding acquisition. **Gil Rilov:** Data Curation, Writing - Review and Editing, Funding acquisition. **António M. Santos:** Data Curation, Writing - Review and Editing. **Lara L. Sousa:** Data Curation, Writing - Review and Editing. **Fernando P. Lima:** Conceptualization, Methodology, Data Curation, Software, Writing - Original Draft and Review and Editing, Supervision, Funding acquisition, Project administration.

Declaration of competing interest

The authors declare that they have no known competing financial interests or personal relationships that could have appeared to influence the work reported in this paper.

Acknowledgements

This work was supported by ERDF funds through COMPETE [grant number POCI-01-0145-FEDER-031088], through PORTUGAL 2020 [PORBIOTA, grant number POCI-01-0145-FEDER-022127], and through POR Norte [grant numbers NORTE-01-0145-FEDER-031053], and by Portuguese national funds through FCT [grant numbers PTDC/BIA-BMA/31088/2017, PTDC/BIA-BMA/31053/2017, PTDC/MAR/121016/2010]. CM was supported by FCT [grant number PD/BD/114038/2015]. RS was supported by NORTE2020 through ERDF [MARINFO, grant number NORTE-01-0145-FEDER-000031]. BRB was funded by FONDECYT [grant number 1181300] and by the Millennium Center for the Study of Multiple-Drivers on Marine Socio-Ecological Systems. BKCC was supported by the Ministry of Science and Technology, Taiwan [grant number MOST-103-2621-B-001-005-MY3]. TGH and GR were funded by the Ministry of Environmental Protection as part of the Israel national monitoring program, Israel Science Foundation [grant number 117/10] and by the Ministry of Science and Technology, Israel, and by the Federal Ministry of Education and Research (BMBF), Germany. DSW was supported by NSF [grant number 1129401] and NASA [grant number NNX11AP77G]. PAR was supported by FCT through QREN and COMPETE [grant number SFRH/BPD/69232/2010]. FES2012 data were produced by Noveltis, Legos and CLS Space Oceanography Division and distributed by Aviso, with support from CNES (<http://www.aviso.altimetry.fr/>). We thank Nuno Queiroz, Sérgio Velho, Ana Gomes, Raquel Xavier, Ricardo Araújo, Signe Nielsen, João Gonçalves, Rita Carriço, Ana Raposo and Gilberto Carreira for their help with field work.

Appendix A. Supplementary data

Supplementary data to this article can be found online at <https://doi.org/10.1016/j.rse.2019.111588>.

References

- Alvarez, I., Gomez-Gesteira, M., deCastro, M., Lorenzo, M.N., Crespo, A.J.C., Dias, J.M., 2011. Comparative analysis of upwelling influence between the western and northern coast of the Iberian Peninsula. *Cont. Shelf Res.* 31, 388–399.
- Baker-Austin, C., Trinanes, J.A., Taylor, N.G.H., Hartnell, R., Siitonen, A., Martinez-Urtaza, J., 2013. Emerging *Vibrio* risk at high latitudes in response to ocean warming. *Nat. Clim. Chang.* 3, 73–77.
- Bakun, A., Field, D.B., Redondo-Rodriguez, A., Weeks, S.J., 2010. Greenhouse gas, upwelling-favorable winds, and the future of coastal ocean upwelling ecosystems. *Glob. Chang. Biol.* 16, 1213–1228.
- Bates, A.E., Helmuth, B., Burrows, M.T., Duncan, M.I., Garrabou, J., Guy-Haim, T., Lima, F., Queiros, A.M., Seabra, R., Marsh, R., 2018. Biologists ignore ocean weather at their peril. *Nature* 560, 299–301.
- Brewin, R., Smale, D., Moore, P., Dall'Olmo, G., Miller, P., Taylor, B., Smyth, T., Fishwick, J., Yang, M., 2018. Evaluating operational AVHRR sea surface temperature data at

- the coastline using benthic temperature loggers. *Remote Sens.* 10, 925.
- Carrère, L., Lyard, F., Cancet, M., Guillot, A., Roblou, L., 2013. FES2012: a new global tidal model taking advantage of nearly 20 years of altimetry. In: *Ouweland, L. (Ed.), 20 Years of Progress in Radar Altimetry, (Venice)*.
- Castillo, K.D., Lima, F.P., 2010. Comparison of in situ and satellite-derived (MODIS-Aqua/Terra) methods for assessing temperatures on coral reefs. *Limnol. Oceanogr. Methods* 8, 107–117.
- Castillo, K.D., Ries, J.B., Weiss, J.M., Lima, F.P., 2012. Decline of forereef corals in response to recent warming linked to history of thermal exposure. *Nat. Clim. Chang.* 2, 756–760.
- Chavez, F.P., Messié, M., 2009. A comparison of eastern boundary upwelling ecosystems. *Prog. Oceanogr.* 83, 80–96.
- Crabbe, M.J.C., 2019. Adapting to extreme environments: can coral reefs adapt to climate change? *Emerg. Top. Life Sci.* 3, 183–195.
- DeCastro, M., Gómez-Gesteira, M., Costoya, X., Santos, F., 2014. Upwelling influence on the number of extreme hot SST days along the Canary upwelling ecosystem. *J. Geophys. Res.-Oceans* 119, 3029–3040.
- Demarcq, H., 2009. Trends in primary production, sea surface temperature and wind in upwelling systems (1998–2007). *Prog. Oceanogr.* 83, 376–385.
- Derrien, M., Farki, B., Harang, L., LeGleau, H., Noyalet, A., Pochic, D., Sairouni, A., 1993. Automatic cloud detection applied to NOAA-11/AVHRR imagery. *Remote Sens. Environ.* 46, 246–267.
- Donlon, C., Minnett, P.J., Gentemann, C., Nightingale, T., Barton, I., Ward, B., Murray, M., 2002. Toward improved validation of satellite sea surface skin temperature measurements for climate research. *J. Clim.* 15, 353–369.
- Donlon, C., Robinson, I., Casey, K.S., Vazquez-Cuervo, J., Armstrong, E., Arino, O., Gentemann, C., May, D., LeBorgne, P., Piollé, J., Barton, I., Beggs, H., Poulter, D.J.S., Merchant, C.J., Bingham, A., Heinz, S., Harris, A., Wick, G., Emery, B., Minnett, P., Evans, R., Llewellyn-Jones, D., Mutlow, C., Reynolds, R.W., Kawamura, H., Rayner, N., 2007. The Global Ocean Data Assimilation Experiment High-resolution Sea Surface Temperature Pilot Project. *Bull. Am. Meteorol. Soc.* 88, 1197–1214.
- Fairall, C., Bradley, E.F., Godfrey, J., Wick, G., Edson, J.B., Young, G.S., 1996. Cool-skin and warm-layer effects on sea surface temperature. *J. Geophys. Res.-Oceans* 101, 1295–1308.
- Flores, C., Gayo, E.M., Salazar, D., Broitman, B.R., 2018. $\delta^{18}\text{O}$ of *Fissurella maxima* as a proxy for reconstructing Early Holocene sea surface temperatures in the coastal Atacama desert (25° S). *Palaeogeogr. Palaeoclimatol. Palaeoecol.* 499, 22–34.
- Freeman, E., Woodruff, S.D., Worley, S.J., Lubker, S.J., Kent, E.C., Angel, W.E., Berry, D.I., Brohan, P., Eastman, R., Gates, L., Gloeden, W., Ji, Z.H., Lawrimore, J., Rayner, N.A., Rosenhagen, G., Smith, S.R., 2017. ICOADS Release 3.0: a major update to the historical marine climate record. *Int. J. Climatol.* 37, 2211–2232.
- Hobday, A.J., Alexander, L.V., Perkins, S.E., Smale, D.A., Straub, S.C., Oliver, E.C., Benthuyesen, J.A., Burrows, M.T., Donat, M.G., Feng, M.J., 2016. A hierarchical approach to defining marine heatwaves. *Prog. Oceanogr.* 141, 227–238.
- Holbrook, N.J., Scannell, H.A., Gupta, A.S., Benthuyesen, J.A., Feng, M., Oliver, E.C., Alexander, L.V., Burrows, M.T., Donat, M.G., Hobday, A.J., 2019. A global assessment of marine heatwaves and their drivers. *Nat. Commun.* 10, 2624.
- Isachsen, P., Koszalka, I., LaCasce, J., 2012. Observed and modeled surface eddy heat fluxes in the eastern Nordic Seas. *J. Geophys. Res.-Oceans* 117, C08020.
- Johnstone, J.A., Dawson, T.E., 2010. Climatic context and ecological implications of summer fog decline in the coast redwood region. *Proc. Natl. Acad. Sci.* 107, 4533–4538.
- Judge, R., Choi, F., Helmuth, B., 2018. Life in the slow lane: recent advances in data logging for intertidal ecology. *Front. Ecol. Evol.* 6, 213.
- Kämpf, J., Chapman, P., 2016. *Upwelling Systems of the World*. Springer International Publishing Switzerland.
- King, W., Sebens, K.P., 2018. Non-additive effects of air and water warming on an intertidal predator-prey interaction. *Mar. Biol.* 165, 64.
- Lafon, V., Martins, A., Bashmachnikov, I., Jose, F., Melo-Rodrigues, M., Figueiredo, M., Mendonca, A., Macedo, L., 2004. SST variability in the Azores region using AVHRR imagery: regional to local scale study. In: *Remote Sensing of the Ocean and Sea Ice 2004*. 5569. pp. 130–139.
- Langlais, C.E., Lenton, A., Heron, S.F., Evenhuis, C., Sen Gupta, A., Brown, J.N., Kuchinke, M., 2017. Coral bleaching pathways under the control of regional temperature variability. *Nat. Clim. Chang.* 7, 839–844.
- Liao, E.H., Lu, W.F., Yan, X.H., Jiang, Y.W., Kidwell, A., 2015. The coastal ocean response to the global warming acceleration and hiatus. *Sci. Rep.* 5, 16630.
- Lima, F.P., Wethey, D.S., 2012. Three decades of high-resolution coastal sea surface temperatures reveal more than warming. *Nat. Commun.* 3, 704.
- Lima, F.P., Burnett, N.P., Helmuth, B., Kish, N., Aveni-Deforge, K., Wethey, D.S., 2011. In: *George, A. (Ed.), Monitoring the intertidal environment with bio-mimetic devices. Biomimetic Based Applications InTech*.
- Lourenço, C.R., Zardi, G.I., McQuaid, C.D., Serrao, E.A., Pearson, G.A., Jacinto, R., Nicastro, K.R.J.J., 2016. Upwelling areas as climate change refugia for the distribution and genetic diversity of a marine macroalga. *J. Biogeogr.* 43, 1595–1607.
- Minnett, P.J., Smith, M., Ward, B., 2011. Measurements of the oceanic thermal skin effect. *Deep-Sea Res. II Top. Stud. Oceanogr.* 58, 861–868.
- O'Carroll, A.G., Armstrong, E.M., Beggs, H., Bouali, M., Casey, K.S., Corlett, G.K., Dash, P., Donlon, C., Gentemann, C.L., Hoyer, J.L., 2019. Observational needs of sea surface temperature. *Front. Mar. Sci.* 6, 420.
- Oliver, E.C., Benthuyesen, J.A., Bindoff, N.L., Hobday, A.J., Holbrook, N.J., Mundy, C.N., Perkins-Kirkpatrick, S.E., 2017. The unprecedented 2015/16 Tasman Sea marine heatwave. *Nat. Commun.* 8, 16101.
- Pauly, D., Christensen, V., 1995. Primary production required to sustain global fisheries. *Nature* 374, 255.
- R Core Team, 2018. *R: A Language and Environment for Statistical Computing*. R Foundation for Statistical Computing, Vienna, Austria.
- Rilov, G., Mazaris, A.D., Stelzenmüller, V., Helmuth, B., Wahl, M., Guy-Haim, T., Mieszkowska, N., Ledoux, J.-B., Katsanevakis, S., 2019. Adaptive marine conservation planning in the face of climate change: what can we learn from physiological, genetic and ecological studies? *Glob. Ecol. Conserv.* 17, e00566.
- Rouault, M., Pohl, B., Penven, P., 2010. Coastal oceanic climate change and variability from 1982 to 2009 around South Africa. *Afr. J. Mar. Sci.* 32, 237–246.
- Santos, F., DeCastro, M., Gómez-Gesteira, M., Álvarez, I., 2012. Differences in coastal and oceanic SST warming rates along the Canary upwelling ecosystem from 1982 to 2010. *Cont. Shelf Res.* 47, 1–6.
- Santos, F., Gómez-Gesteira, M., Varela, R., Ruiz-Ochoa, M., Días, J., 2016. Influence of upwelling on SST trends in La Guajira system. *J. Geophys. Res.-Oceans* 121, 2469–2480.
- Schlegel, R.W., Oliver, E.C.J., Wernberg, T., Smit, A.J., 2017. Nearshore and offshore co-occurrence of marine heatwaves and cold-spells. *Prog. Oceanogr.* 151, 189–205.
- Seabra, R., Wethey, D.S., Santos, A.M., Lima, F.P., 2011. Side matters: microhabitat influence on intertidal heat stress over a large geographical scale. *J. Exp. Mar. Biol. Ecol.* 400, 200–208.
- Seabra, R., Wethey, D.S., Santos, A.M., Lima, F.P., 2015. Understanding complex biogeographic responses to climate change. *Sci. Rep.* 5, 12930.
- Seabra, R., Wethey, D.S., Santos, A.M., Gomes, F., Lima, F.P., 2016. Equatorial range limits of an intertidal ectotherm are more linked to water than air temperature. *Glob. Chang. Biol.* 22, 3320–3331.
- Seabra, R., Varela, R., Santos, A.M., Gomez-Gesteira, M., Meneghesso, C., Wethey, D.S., Lima, F.P., 2019. Reduced nearshore warming associated with eastern boundary upwelling systems. *Front. Mar. Sci.* 6, 104.
- Smale, D.A., Wernberg, T., 2009. Satellite-derived SST data as a proxy for water temperature in nearshore benthic ecology. *Mar. Ecol. Prog. Ser.* 387, 27–37.
- Smit, A.J., Roberts, M., Anderson, R.J., Dufois, F., Dudley, S.F., Bornman, T.G., Olbers, J., Bolton, J.J., 2013. A coastal seawater temperature dataset for biogeographical studies: large biases between in situ and remotely-sensed data sets around the coast of South Africa. *PLoS One* 8, e81944.
- Strub, P., Mesías, J., Montecino, V., Rutllant, J., Salinas, S., 1998. Coastal ocean circulation off western South America Coastal segment (6, E). In: *The Sea*. 11. pp. 273–313.
- Tapia, F.J., Navarrete, S.A., Castillo, M., Menge, B.A., Castilla, J.C., Largier, J., Wieters, E.A., Broitman, B.L., Barth, J.A., 2009. Thermal indices of upwelling effects on inner-shelf habitats. *Prog. Oceanogr.* 83, 278–287.
- Taylor, K.E., 2001. Summarizing multiple aspects of model performance in a single diagram. *J. Geophys. Res.* 106, 7183–7192.
- Thakur, K.K., Vanderstichel, R., Barrell, J., Stryhn, H., Patanasatienkul, T., Revie, C.W., 2018. Comparison of remotely-sensed sea surface temperature and salinity products with in situ measurements from British Columbia, Canada. *Front. Mar. Sci.* 5, 121.
- Vancamp, L., Nykjaer, L., Mittelstaedt, E., Schlittenhard, P., 1991. Upwelling and boundary circulation off Northwest Africa as depicted by infrared and visible satellite-observations. *Prog. Oceanogr.* 26, 357–402.
- Varela, R., Alvarez, I., Santos, F., deCastro, M., Gomez-Gesteira, M., 2015. Has upwelling strengthened along worldwide coasts over 1982–2010? *Sci. Rep.* 5.
- Varela, R., Lima, F.P., Seabra, R., Meneghesso, C., Gómez-Gesteira, M., 2018. Coastal warming and wind-driven upwelling: a global analysis. *Sci. Total Environ.* 639, 1501–1511.
- Vazquez-Cuervo, J., Dewitte, B., Chin, T.M., Armstrong, E.M., Purca, S., Alburqueque, E., 2013. An analysis of SST gradients off the Peruvian Coast: the impact of going to higher resolution. *Remote Sens. Environ.* 131, 76–84.
- Vazquez-Cuervo, J., Torres, H.S., Menemenlis, D., Chin, T., Armstrong, E.M., 2017. Relationship between SST gradients and upwelling off Peru and Chile: model/satellite data analysis. *Int. J. Remote Sens.* 38, 6599–6622.